



Structure and dehydration of layered perovskite niobate with bilayer hydrates prepared by exfoliation/self-assembly process

Yufeng Chen^{a,b}, Xinhua Zhao^a, Hui Ma^c, Shulan Ma^a, Gailing Huang^a, Yoji Makita^d, Xuedong Bai^e, Xiaojing Yang^{a,*}

^a College of Chemistry, Beijing Normal University, Beijing 100875, China

^b Department of Chemistry, Nanchang University, Jiangxi 330031, China

^c Analysis and Test Center, Beijing Normal University, Beijing 100875, China

^d National Institute of Advanced Industrial Science and Technology, 2217-14 Hayashi, Takamatsu 761-0395, Japan

^e Institute of Physics, Chinese Academy of Sciences, Beijing 100080, China

ARTICLE INFO

Available online 12 June 2008

Keywords:

Self-assembly

Exfoliation

Layered perovskite niobate

Nanosheet

ABSTRACT

The crystals of an H-form niobate of $\text{HCa}_2\text{Nb}_3\text{O}_{10} \cdot x\text{H}_2\text{O}$ ($x = 0.5$) being tetragonal symmetry (space group $P4/mbm$) with unit cell parameters $a = 5.4521(6)$ and $c = 14.414(2)$ Å were exfoliated into nanosheets with the triple-layered perovskite structure. The colloid suspension of the nanosheets was put into dialysis membrane tubing and allowed self-assembly in a dilute KCl solution. By this method, a novel layered K-form niobate $\text{KCa}_2\text{Nb}_3\text{O}_{10} \cdot x\text{H}_2\text{O}$ ($x = 1.3$, typically) with bilayer hydrates in the interlayer was produced. The Rievel refinement and transmission electron microscope (TEM)/selected-area electron diffraction (SAED) observation indicated that the orientations of the a -/ b -axis of each nanosheet as well as the c -axis are uniform, and the self-assembled compound had the same symmetry, tetragonal ($P4/mbm$) with $a = 5.453(2)$ and $c = 16.876(5)$ Å, as the H-form precursor; the exfoliation/self-assembly process does not markedly affect the two-dimensional lattice of the layer. The large basal spacing resulted from the interlayer K^+ ions solvated by two layers of water molecules. The interlayer bilayers-water was gradually changed to monolayer when the temperatures higher than 100 °C, and all the water molecules lost when over 600 °C. Accompanying the dehydration, the crystal structure transformed from tetragonal to orthorhombic symmetry. Water molecules may take an important role for the layer layered compound to adjust the unit cell to tetragonal symmetry.

© 2008 Elsevier Inc. All rights reserved.

1. Introduction

Cation-exchangeable transition-metal layered oxides are layered compounds with particularly interesting and variable characteristics, such as thermoelectricity [1], piezoelectricity [2], photocatalytic property [3], ferroelectricity [4], etc. These compounds consist of polyanion sheets of transition-metal oxides with alkaline metal cations in the interlayers. The negatively charged metal oxide sheets function as host structure for ion-exchange reaction of alkaline metal cations with various other cations, as well as for the intercalation of poly-ions/small molecules. Some researches on the intercalation and exfoliation of these layered compounds have been actually carried out, such as titanate [5], manganese oxide [6], graphite oxide [7], phosphate [8], niobate [3b,9], etc. In particular, the exfoliation of layered niobates exemplified by $\text{K}_4\text{Nb}_6\text{O}_{17}$, HTiNbO_5 , and $\text{HCa}_2\text{Nb}_3\text{O}_{10}$ has been paid attention because of the potential applica-

tion for advanced materials with the utility of their photoactive nature [10] and capability of organizing guest species on the layer surface [11].

The nanosheets, called inorganic supermolecules or two-dimensional crystals, obtained by exfoliation of metal oxides exist in a colloid suspension state with their, usually, organic solution. The restacking using nanosheets as building blocks to reconstruct new structures has been reported [12]. The studies are mainly focused on the layer-by-layer method [12b–d,13]. For example, since $\text{HCa}_2\text{Nb}_3\text{O}_{10}$ and $\text{KCa}_2\text{Nb}_3\text{O}_{10}$ possess some interesting properties, such as photo catalysts [14] and hydrogen sensor [15], some groups have researched on the self-assembly of the $\text{Ca}_2\text{Nb}_3\text{O}_{10}^-$ nanosheets. Mallouk et al. have reported the multi-layer thin films of $\text{Ca}_2\text{Nb}_3\text{O}_{10}^-$ nanosheets prepared by layer-by-layer method [12b–d]. Ebina et al. have exfoliated the layered $\text{HCa}_2\text{Nb}_3\text{O}_{10} \cdot 1.5\text{H}_2\text{O}$ with tetrabutylammonium (TBA^+) and restacked the nanosheets into precipitate by flocculation [12a,16]. The basal spacing of the precipitate was found to be ca.17 Å, about 2 Å larger than that of the starting compound of $\text{KCa}_2\text{Nb}_3\text{O}_{10}$. The phase was explained as maybe due to hydration [12a],

* Corresponding author. Fax: +86 10 5880 2075.

E-mail address: yang.xiaojing@bnu.edu.cn (X. Yang).

however, has not been studied further. It is actually difficult to investigate the structure in detail since restacked samples have usually high orientation in the direction perpendicular to the layers but very low crystallinity in other directions. To obtain a self-assembled potassium niobate with high crystallinity, in this study we use a method with dialysis membrane tubing and diluted salt solution, by which we have studied the self-assembly of MnO_2 nanosheets [17], and found that it provides an exceedingly mobile environment for nanosheets to freely reach a regular structure.

Two types of structures are found in self-assembled layered compounds, namely a turbostratic structure with the *a*- or *b*-axis of each nanosheet in random orientation along the *c*-axis (the direction of layers) [18], and another structure [17] with the *a*- or *b*-axis of each nanosheet in azimuthal orientation along the *c*-axis. In the present study, starting from triple-layered perovskite $\text{KCa}_2\text{Nb}_3\text{O}_{10}$, after protonation and exfoliation/self-assembly process, a compound with K^+ ions solvated by two layers of water molecules is obtained. Its intralayer structure had the *a*- or *b*-axis of each nanosheet in the same orientation, reconstructing to the structure of its protonated precursor. In its interlayer, the structure of bilayer hydrates is analogous to some layered compounds with brucite layers, such as busenite-type manganese oxides [19], the superconducting $\text{Na}_x\text{CoO}_2 \cdot y\text{H}_2\text{O}$ [20] and $\text{Na}_{0.3}\text{NiO}_2 \cdot 1.3\text{H}_2\text{O}$ [21], but for layered perovskite structures, to our best knowledge, has not been refined before.

2. Experimental section

2.1. Exfoliation of protonated $\text{KCa}_2\text{Nb}_3\text{O}_{10}$

Layered perovskite, $\text{KCa}_2\text{Nb}_3\text{O}_{10}$ (abbreviated as K-form sample) was prepared by solid-state reaction method as reported in the literature [22]. The reagents K_2CO_3 , CaCO_3 , and Nb_2O_5 (obtained from Chemical Plant of Beijing, Chemistry Reagent Corporation of Beijing, Chemistry Reagent Corporation of National Medicine Group, respectively) were mixed and then water was added to make the mixture into a paste. The paste was dried at 90–110 °C to give a powder, and then the powder was put into a platinum crucible and heated at 1200 °C for 12 h. The product was water-washed and dried at 110 °C overnight. The protonation of K-form sample (2.0 g) was performed by soaking in 50 cm³ of a HNO_3 aqueous solution (6 M), stirred for 48 h, and then filtered, water-washed, and dried at 110 °C. The obtained sample is noted as H-form sample.

A colloidal suspension was obtained by adding a specific amount of H-form powder (0.5 g) in 200 cm³ of a tetramethylammonium hydroxide (TMAOH) aqueous solution at a molar ratio of $\text{TMAOH}/\text{HCa}_2\text{Nb}_3\text{O}_{10} = 10$, and stirred at room temperature for about 15 days.

2.2. Self-assembly via dilute salt dialysis process

The colloidal nanosheet suspension was diluted to 1.27 g dm⁻³ and put into molecular-porous dialysis membrane tubing (obtained from Shanghai Green Bird Science & Technology Development Co. Ltd.). The tubing was soaked in a 5 mmol dm⁻³ KCl aqueous solution (2 dm³). After soaking for 2 days, the supernatant solution in the tubing became clear. The precipitate was filtrated, water-washed, and dried at 70 °C. The obtained sample is referred as to self-assembled sample. Measurement of pH and electron conductivity of the KCl solution during this process indicated that the method allowed the self-assembly

process to take place slowly, and consequently the restacked crystals had high crystallinity.

2.3. Characterization technique

Powder X-ray diffraction (XRD) patterns were collected using a Phillips X'pert Pro MPD diffractometer with $\text{CuK}\alpha$ radiation. The generator setting is 40 kV and 40 mA. The XRD patterns of the K-form, H-form, and self-assembled compounds were measured at room temperature with step size of 0.017 °, scan time of 20 s per

Table 1
Compositions of H-type and self-assembled compounds

Sample	Content ^a (mg g ⁻¹)			Weight loss ^b (%)	Formula
	K	Ca	Nb		
H-type	0	149	527	3.46	$\text{HCa}_2\text{Nb}_{3.04}\text{O}_{10.1} \cdot 0.5\text{H}_2\text{O}$
Self-assembled	67	137	479	4.22	$\text{KCa}_{1.99}\text{Nb}_{2.99}\text{O}_{9.96} \cdot 1.3\text{H}_2\text{O}$

^a Analyzed by ICP.

^b Obtained from the TG curves, 25–600 °C.

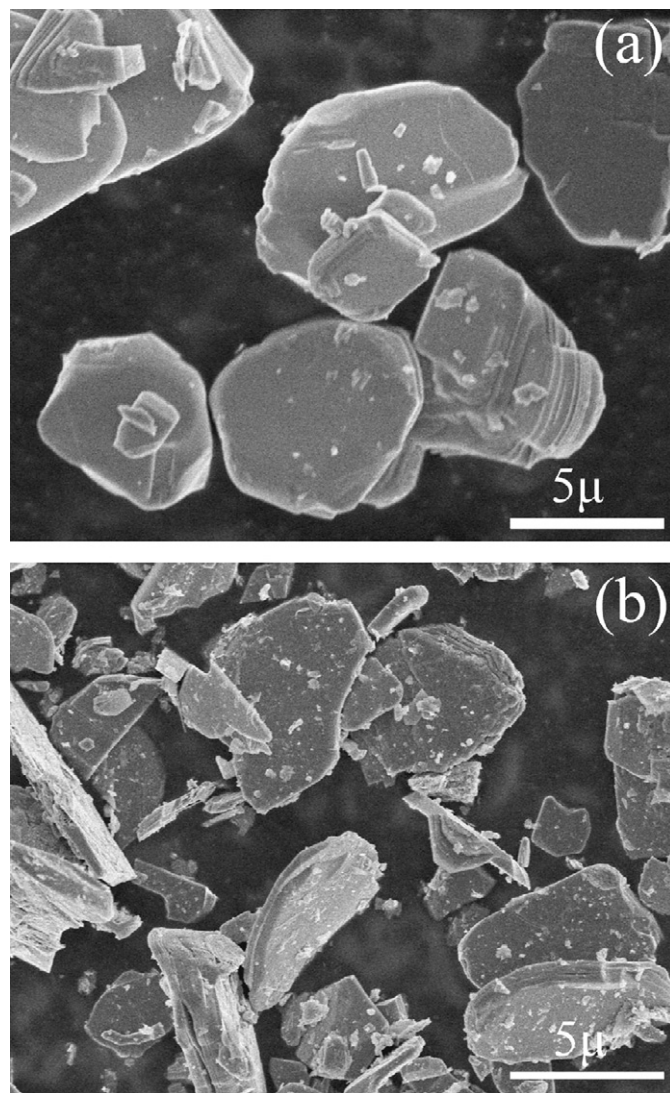


Fig. 1. Scanning electron microscope images of (a) starting material $\text{KCa}_2\text{Nb}_3\text{O}_{10}$ compared with (b) H-form sample.

step, and 2θ ranging from 4.5° to 120° . Rietveld refinements were performed by the combination of the Rietveld analysis, maximum-entropy method (MEM) and MEM-based pattern fitting [23], using the software RIETAN-2000 [23c].

To detect the thermal stability of the self-assembled sample at various temperatures, their XRD data were collected *in situ* with the conditions: step size, 0.017° ; scan step time, 15 s; temperature ascending speed, $30^\circ\text{C min}^{-1}$; heat preservation time at each selected temperature, 3 min; and 2θ range, 4.5° to 80° . The temperature was increased in 20°C steps from 40 to 600°C . The change of temperature was controlled by the TCU2000 Temperature Control Unit (Anton Parr Co.).

Thermal gravimetric (TG) and differential thermal analysis (DTA) data were collected using SDT Q600 V8.0 Build 95 thermal

analyzer. The sample was put into Pt crucible and with heating rate of $10^\circ\text{C min}^{-1}$ in air ambient.

Fourier Infrared spectra of the samples were recorded on a Nicolet-380 Fourier-transform infrared spectrometer using the KBr method.

Chemical composition of K, Ca, and Nb were determined by inductively coupled plasma (ICP) atomic emission spectroscopy (Jarrel-ASH, ICAP-9000). A weighted amount of the niobate was dissolved with a mixed acid solution of 10 cm^3 concentrated HNO_3 and 2 cm^3 concentrated HF by heating it at $90\text{--}100^\circ\text{C}$ in a Pt crucible and was evaporated to remove excess HF, and then 9 M H_2SO_4 was added. While still warm, the solution was put into a flask with oxalic acid and water. The chemistry formula was calculated from the results of ICP and TG analysis.

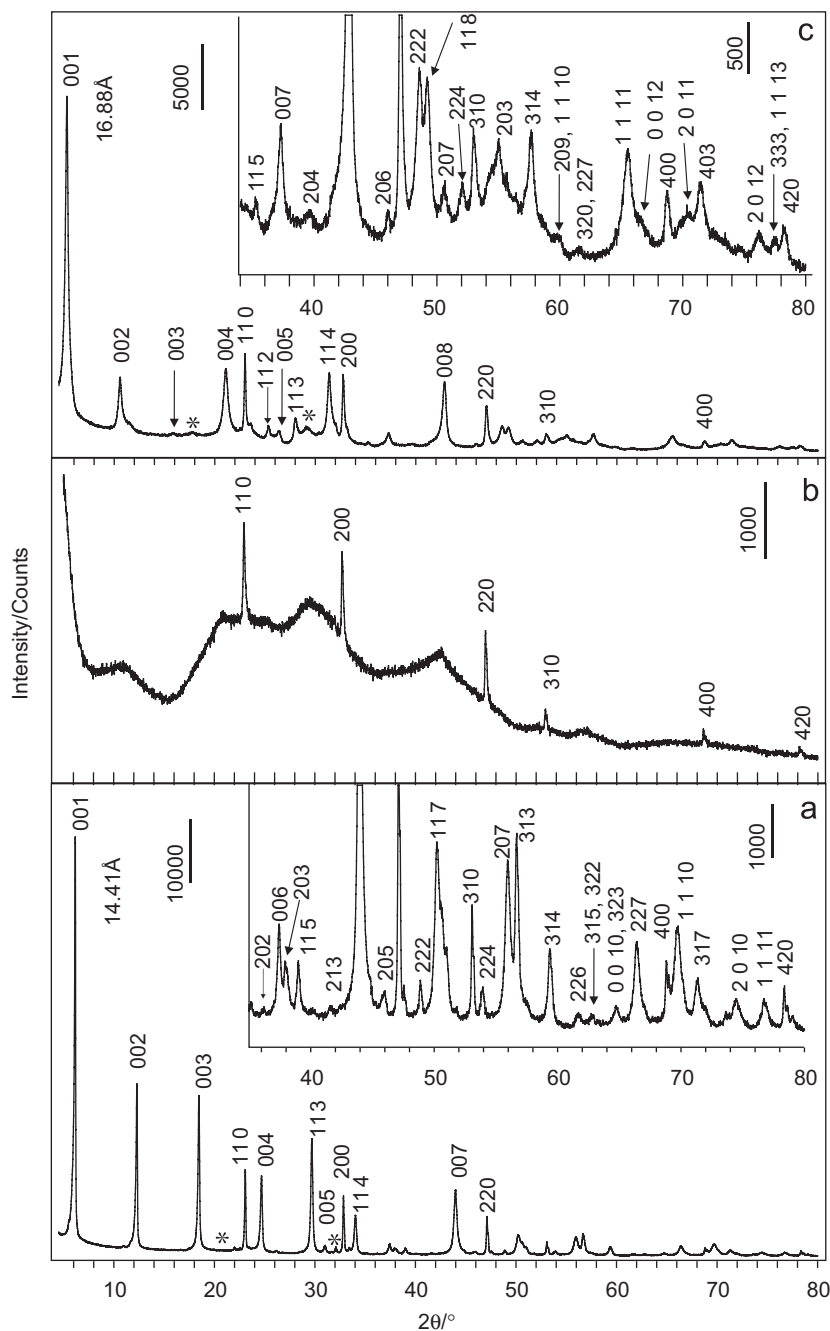


Fig. 2. XRD patterns of the samples (a) H-form niobate, (b) in wet state after H-form niobate soaked in TMAOH solution for about 15 days and then centrifugated, and (c) the self-assembled one.

High-resolution transmission electron microscope (TEM) and selected-area electron diffraction (SAED) observations were performed using a JEM-2010F (JEOL Ltd.) at an accelerating voltage of 200 kV. Scanning electron microscope (SEM) observation was carried out using a mode S-4800 (Hitachi, Ltd.) operating at 5.0 kV.

The nanosheets were observed by an atomic force microscope (AFM, Nanoscope IIIA multimode, Veeco Metrology Group) and SEM after restacking on a Si wafer by the layer-by-layer method. The specimen was prepared as following. Polished Si (111) wafer (*n*-type) was cleaned with acetone, rinsed with methanol and deionized water, respectively, and then dried by high pure N₂ gas. The sample of Ca₂Nb₃O₁₀⁻/PEI/Si was obtained by layer-by-layer method. The Si wafer was primed by a treatment with a polyethylenimine solution (PEI, *M_w*~750,000; 1.08 g dm⁻³) for 20 min to introduce a positive charge to the wafer surface. The wafer was deposited into a suspension of the Ca₂Nb₃O₁₀⁻ (0.7 g dm⁻³) and after 20 min, the excess Ca₂Nb₃O₁₀⁻ sheets and other ions were removed thoroughly by water-washing.

3. Results and discussion

3.1. Structural change from *K*- to *H*-type niobate crystals

The chemical formula of the *H*-form sample was analyzed to be HCa₂Nb₃O₁₀·0.5H₂O (Table 1), indicating that all K⁺ ions were extracted from starting material KCa₂Nb₃O₁₀ by H⁺/K⁺ ion exchange and water molecules were intercalated into the interlayer. The SEM images show that the *H*-form sample (Fig. 1b) remains the morphology of its precursor (Fig. 1a), where the particles are composed of plates. The XRD patterns show that the change of the interlayer guest species results in the decrease of the basal spacing, *d*_{basal}, from 14.62 Å of *K*-form (Fig. S2, supplementary data) to 14.41 Å of *H*-form (Fig. 2a).

Furthermore, the crystal symmetry is changed, from an orthorhombic structure to the tetragonal symmetry after the interlayer guest species is changed by the soft-chemistry method. For KCa₂Nb₃O₁₀, tetragonal [24] and orthorhombic [25] were reported to describe the structures. Our present result of a Rietveld refinement showed it was orthorhombic (space group,

Cmcm) with *a* = 3.8802(9), *b* = 29.508(6), and *c* = 7.714(1) Å (Table S1, Fig. S2 and S3, supplementary data), the same as that of Fukuoka et al. [25]. For the *H*-form HCa₂Nb₃O₁₀·0.5H₂O, as shown in Fig. 2a, all the reflection peaks except for two small ones at 2θ = 32.3° and 23.6°, possibly due to impurity [26], can be indexed to tetragonal (space group *P4/mbm*). A Rietveld refinement was carried out [23], when we introduced a fiction species of WO, whose atomic scattering factors were set equal to the sums of those of one O and four H atoms according to the composition. The patterns and final structure parameters are given in Fig. 3 and Table 2, respectively. The unit cell parameters, *a* = 5.4521(6) and *c* = 14.414(2) Å, are different from the results of Jacobson et al., *a* = 3.851 and *c* = 14.38 Å for HCa₂Nb₃O₁₀ [24b], and *a* = 3.849 and *c* = 16.21 Å for HCa₂Nb₃O₁₀·*x*H₂O (*x* = 1–1.5) [27]. For those compounds, the *a* value is equal to Nb···Nb distance, whereas the large *a* value in our compound is √2 times of Nb···Nb distance. This may be caused by the large deviation of the inter-octahedral Nb–O–Nb angles (143.7(3)° for central NbO₆ octahedra, and 152.4(2)° for terminal octahedra) from the ideal value of 180° in the *ab* plane [27], thus leading to the angular change between NbO₆ octahedra, as shown in Fig. 4b.

The low occupancy and the Wyckoff position of WO species (Table 2) show that H₂O or H₃O⁺ is dispersed in the interlayer. It is in 4*f* site close to terminal oxygen atoms of the layer rather than in the middle of the interlayer (2*c* site), giving a interatomic distance

Table 2
Structure parameters of the *H*-form sample HCa₂Nb₃O₁₀·0.5H₂O

Atom	Wyckoff index	<i>g</i>	<i>x</i>	<i>y</i>	<i>z</i>	<i>U</i>
Nb1	2 <i>a</i>	1	0	0	0	0.0062(8)
Nb2	4 <i>e</i>	1	0	0	0.2935(1)	0.0062(8)
O1	4 <i>e</i>	1	0	0	0.1276(6)	0.018(2)
O2	4 <i>e</i>	1	0	0	0.4218(6)	0.018(2)
O3	4 <i>g</i>	1	0.332(3)	0.832(3)	0	0.018(2)
O4	8 <i>k</i>	1	0.270(3)	0.770(3)	0.2624(5)	0.018(2)
Ca1	4 <i>f</i>	1	0	1/2	0.1500(3)	0.014(1)
WO1	4 <i>f</i>	0.37	0	1/2	0.527(2)	0.018(2)

Space group: *P4/mbm* (no. 127); *a* = 5.4521(6) Å, *c* = 14.414(2) Å, *V* = 428.44(8) Å³; virtual species WO, whose atomic scattering factors were set equal to the sums of those of one O and four H atoms. *R*_{wp} = 7.94%, *R*_p = 5.82%, *R*_R = 15.89%, *R*_e = 2.59%, *S* = 3.06.

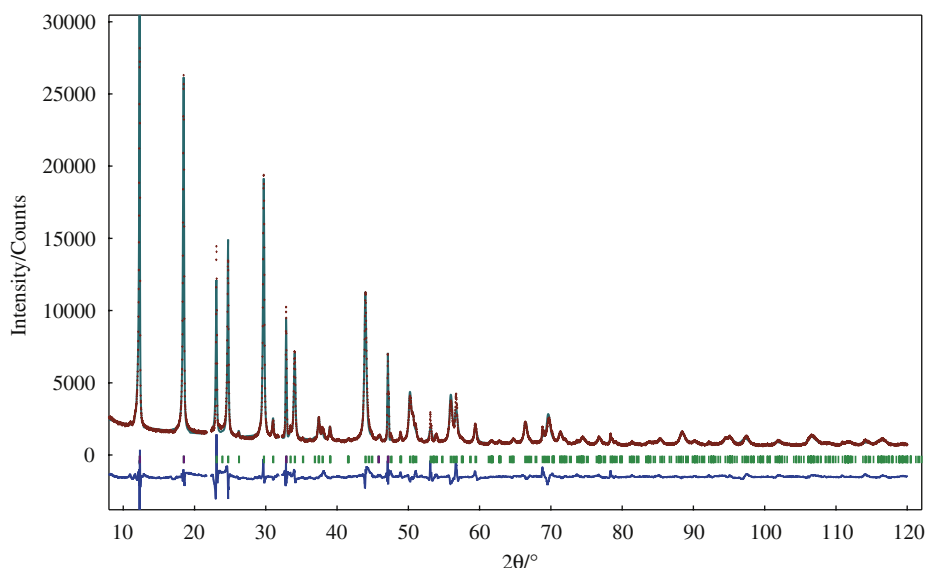


Fig. 3. Rietveld refinement pattern for the *H*-form sample HCa₂Nb₃O₁₀·0.5H₂O. Observed (red crosses), calculated (smooth green line) and their difference (blue trace). The tick marks indicate the positions of allowed Bragg reflections.

WO–O2 2.824(8) Å (Fig. 4). The distance is usually found in oxides such as bilayer-hydrate phase $\text{Na}_{0.42}\text{CoO}_2$ (WO–O 2.68(3) Å) [20b] and $\text{Na}_{0.3}\text{NiO}_2 \cdot 1.3\text{H}_2\text{O}$ (WO–O 2.996(32) Å) [21b]. Comparison with that of K^+ -form sample, the interlayer change in guest species leads to the weakness of the NbO_6 octahedral distortion (Table 4), providing the layer shift from ABAB... to AA... stacking.

3.2. Exfoliation of protonated niobate

The colloid suspension obtained after intercalation reaction of TMA^+ and the H-form sample was centrifugated at 12,000 rpm and subjected to the XRD measurement in wet state. Fig. 2b displays a wavy and broad curve. Besides the broad profile, sharp Bragg reflections corresponding to (110), (200), (220), (310), (400), and (420) planes for $\text{HCa}_2\text{Nb}_3\text{O}_{10} \cdot 0.5\text{H}_2\text{O}$ (Fig. 2a) were observed; while the strong reflections corresponding to (001), (002), and (003) vanished. This indicates that the periodicity for layer-to-layer registry lost and the two-dimensional lattice of the layer was retained when being exfoliated. The reflections attributed to the layer lattice were also observed after being exfoliated to nanosheets in previous work [16a]. The nanosheets less than 3 nm in thickness were detected by the AFM for the sample nanosheet/PEI/Si wafer by the layer-by-layer method (Fig. 5). Fig. 6a shows the SEM image on the sample dried on Si wafer surface. Some of nanosheets were scrolled, showing that they are very thin, as observed by Schaak et al. for nanoscale scrolls formed from exfoliated $\text{H}_2\text{La}_2\text{Ti}_3\text{O}_{10}$ [12c]. The results above indicate that TMA^+ intercalation can also result in exfoliation of the H-form niobate to $\text{Ca}_2\text{Nb}_3\text{O}_{10}$ nanosheets, usually obtained by tetrabutylammonium (TBA^+) [12d,16a].

3.3. Structure of self-assembled compound from $\text{Ca}_2\text{Nb}_3\text{O}_{10}^-$ nanosheets

By treating the colloidal suspension of nanosheets in a dilute KCl solution followed by water-washing and drying, a self-

assembled sample was obtained. In its XRD pattern (Fig. 2c), a strong peak at $2\theta = 5.29^\circ$ ($d = 16.88$ Å) much higher than others shows that the nanosheets are well-restacked, agreeing with the flat particle shape observed by SEM (Fig. 6b). The peaks are indexable on tetragonal symmetry with space group $P4/mbm$. In Fig. 2c, the reflection peaks of the (110), (200), (220), (310), (400), and (420) are produced by two-dimensional lattice in the nanosheets, as observed in the pattern of the exfoliated sample (Fig. 2b). The peaks are still sharper than those of other planes including peaks of (00 l) planes, indicating that the crystallinity of these planes are higher than that of others. Thus in a Rietveld refinement of the pattern, these peaks were not included. The composition of the sample is analyzed to be $\text{KCa}_2\text{Nb}_3\text{O}_{10} \cdot 1.3\text{H}_2\text{O}$

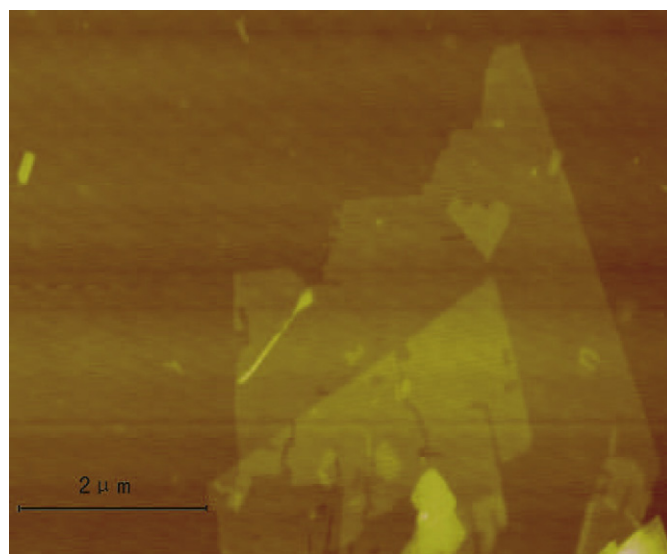


Fig. 5. Tapping-mode atomic force microscopy image of the nanosheets.

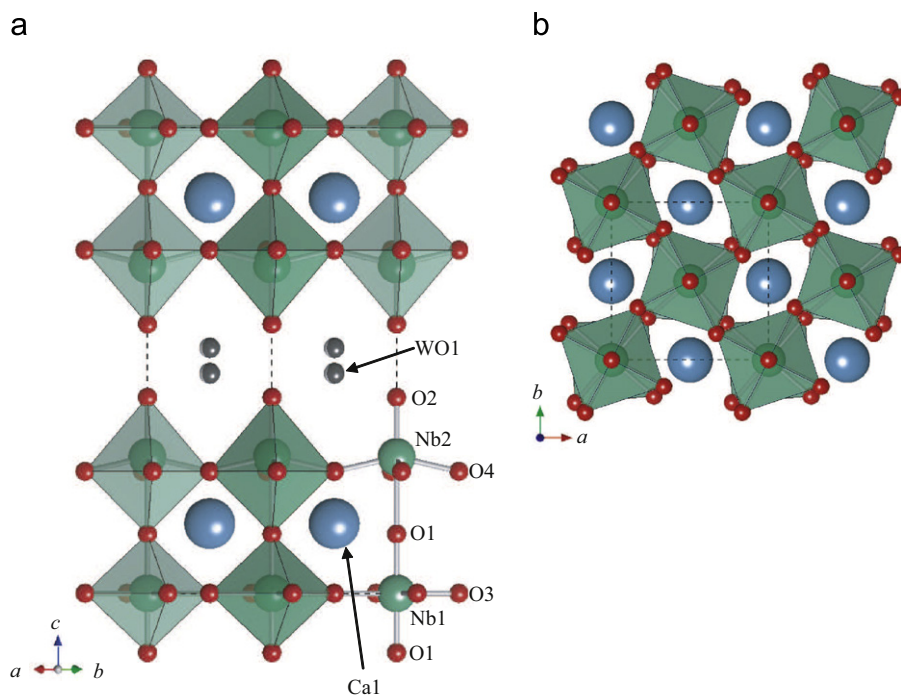


Fig. 4. Polyhedral representations of $\text{HCa}_2\text{Nb}_3\text{O}_{10} \cdot 0.5\text{H}_2\text{O}$, in the directions of [110] (a) and [001] (b). The dashed black line indicates the unit cell. Selected interatomic distances (in Å): Nb1–O1, 1.839(9); Nb1–O3, 2.03(2); Nb2–O1, 2.391(9); Nb2–O2, 1.849(9); Nb2–O4, 1.99(2); Nb1–Nb1 and Nb2–Nb2, 3.8552(3); Nb1–Nb2, 4.231(2); and WO1–O2, 2.824(8).

(Table 1), which means all the negative charge of layered perovskite is compensated by K^+ ions instead of H^+ or other cations, such as TMA^+ .

The lattice parameters of $KCa_2Nb_3O_{10} \cdot 1.3H_2O$ are $a = 5.453(2)$ and $c = 16.876(5)$ Å, as shown in the Rietveld refinement results of Table 3 and Figs. 7 and 8 illustrates the crystal structure. The interlayer space is accommodated by two layers of water molecules and the K^+ ions solvated by them. Such a bilayer-hydrate interlayer structure is also found in the layered compounds with brucite-layers, such as busenite-type manganese oxide [28], the superconducting cobalt oxide of $Na_xCoO_2 \cdot yH_2O$ [20b,21b], $Na_{0.3}NiO_2 \cdot 1.3H_2O$ [21a,29], and hydrated chalcogenides with alkali ions $A_x(H_2O)_z[MX]_2$ [30]. The interlayer guest gallery swells the layered structure leading to the large d_{basal} (16.876(5) Å), being very close to the restacked one (17 Å) reported by Ebina et al. [12a]. A hydrated triple perovskite niobate $NaCa_2Nb_3O_{10} \cdot 2H_2O$ with $d_{basal} = 16.83$ Å has been prepared by Na/Rb ion exchange of $RbCa_2Nb_3O_{10}$ using a $NaNO_3$ flux at 340 °C [31], but the structure is unclear. The a parameter (5.4521(6) Å) of the self-assembled crystals is very close to that of its H-form precursor, $a = 5.453(2)$ Å, being $\sqrt{2}$ times of Nb...Nb distance. The Nb–O–Nb angle of the central NbO_6 octahedron ($147.0(4)^\circ$) is responsible for the large a value. This implies that the exfoliation and restacking process does not markedly affect on the two-dimensional lattice of the layer.

The crystal symmetry and space group of self-assembled sample are the same as the H-form $HCa_2Nb_3O_{10} \cdot 0.5H_2O$ sample, though the interlayer galleries are different. It means that the influence of K^+ ions on the layer is slight when they are solved by bilayers of water molecules. There exist two sites of Nb atoms in the self-assembled crystals, as in K-form and H-form. That is, there are two kinds of NbO_6 octahedra, the central $Nb(1)O_6$ and terminal $Nb(2)O_6$. The average values of Nb(1)–O and Nb(2)–O bond lengths for the self-assembled sample are, respectively, 2.03 and 1.93 Å, while 1.96 and 2.03 for H-form, 1.884 and 2.000 Å for K-form, respectively. These bond lengths are close to the Nb–O bond length of 1.978 Å expected [32] from the bond-valence parameter (1.911) and oxidation number (5) of Nb, and the observed values in the literatures [25,33]. As found in many $n = 3$ members of Dion–Jacobson phase and Ruddlesden–Popper phases, terminal $Nb(2)O_6$ octahedra of triple octahedral layers are strongly distorted while central $Nb(1)O_6$ octahedra are relatively regular. From the Nb–O bond lengths of the present three samples shown in Figs. 4 and 8 and Fig. S3 of supplementary data, respectively, the bond length distortion index (D) [34] and bond angle variance (σ^2) [35] are calculated by Eqs. (1) and (2), respectively, and the results are listed in Table 4:

$$D = \frac{1}{n} \sum_{i=1}^n \frac{|l_i - l_{av}|}{l_{av}} \quad (1)$$

where n is the coordination number of the central atom, l_i the distance from the central atom to the i th coordinating atom, and l_{av} the average bond length:

$$\sigma^2 = \frac{1}{m-1} \sum_{i=1}^m (\varphi_i - \varphi_0)^2 \quad (2)$$

where m is the number of bond angles, equal to 3/2 times of the number of faces in the polyhedron, φ_i is the i th bond angle, and φ_0 the ideal bond angle for a regular polyhedron (90° for an octahedron). The D value of the terminal $Nb(2)O_6$ octahedron is obviously larger than that of the central $Nb(1)O_6$ octahedron in all the three compounds. The D and σ^2 values of both the terminal $Nb(2)O_6$ and central $Nb(1)O_6$ in the self-assembled sample are smaller than those of the corresponding values for other two samples. These results indicate that the bilayer hydrates allow

Nb–O bonds to adjust more freely forming a high symmetric NbO_6 octahedron, thus the self-assembled sample has the same crystal symmetry as that of H-form, rather than the orthorhombic of the K-form sample. In addition, the σ^2 of terminal NbO_6 for H-form is obviously larger than that of the K-form. The different

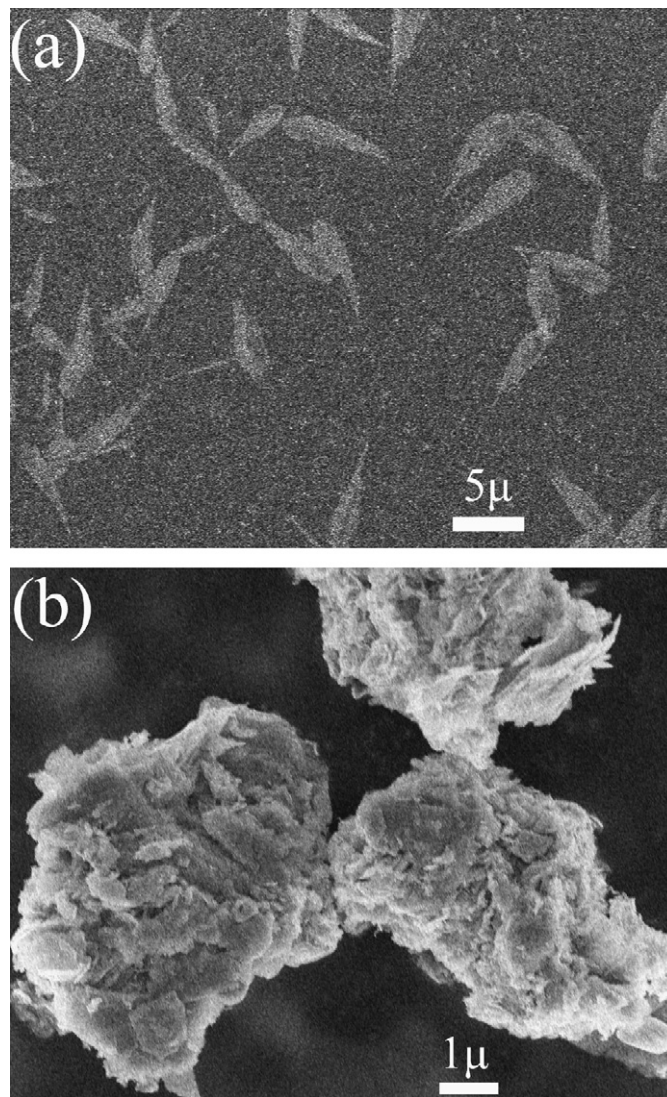


Fig. 6. Scanning electron microscope images of (a) $Ca_2Nb_3O_{10}$ nanosheets and (b) self-assembled compound $KCa_2Nb_3O_{10} \cdot 1.3H_2O$.

Table 3
Structure parameters of the self-assembled compound $KCa_2Nb_3O_{10} \cdot 1.3H_2O$

Atom	Wyckoff index	g	ψ	y	z	U
Nb1	2a	1	0	0	0	0.008(1)
Nb2	4e	1	0	0	0.2501(2)	0.008(1)
O1	4e	1	0	0	0.123(1)	0.008(1)
O2	4e	1	0	0	0.3492(9)	0.008(1)
O3	4g	1	0.324(4)	0.824(4)	0	0.008(1)
O4	8k	1	0.254(8)	0.754(8)	0.2367(8)	0.008(1)
Ca1	4f	1	0	1/2	0.1343(4)	0.008(1)
K1	2b	0.41	0	0	1/2	0.052(9)
K2	4h	0.297	0.342(7)	0.842(7)	1/2	0.052(9)
WO1	4f	0.685	0	1/2	0.588(1)	0.052(9)

Space group: $P4/mbm$ (no. 127); $a = 5.453(2)$ Å, $c = 16.876(5)$ Å, $V = 501.8(3)$ Å³; virtual species WO, whose atomic scattering factors were set equal to the sums of those of one O and two H atoms. $R_{wp} = 8.86\%$, $R_p = 6.81\%$, $R_R = 23.04\%$, $R_e = 2.93\%$, $S = 3.02$.

inter-actions of interlayer H^+ and H_3O^+ on the terminal NbO_6 possibly cause the larger distortion of bond angle than in other form samples.

The TEM micrograph and SAED pattern of the H-form and self-assembled samples are given in Fig. 9. The SAED pattern corresponds to [001] orientation for both of the H-form and self-assembled compounds. For the self-assembled sample, the bright spots corresponding to (110), (020), and $(\bar{1}10)$ planes (Fig. 9b)

suggest that the nanosheets are restacked in the same crystallographic orientation along the c -axis. As the sample was inclined by some degrees, for example $x = -15^\circ, y = 0^\circ$; or $x = 0^\circ, y = 15^\circ$, elliptical diffraction patterns (oblique texture patterns) were not observed (Supplementary data, Fig. S4). Those oblique texture patterns are generally observed at a polycrystalline thin film having a particular crystal axis aligned along a certain direction, with a random arrangement of azimuthal orientation about this

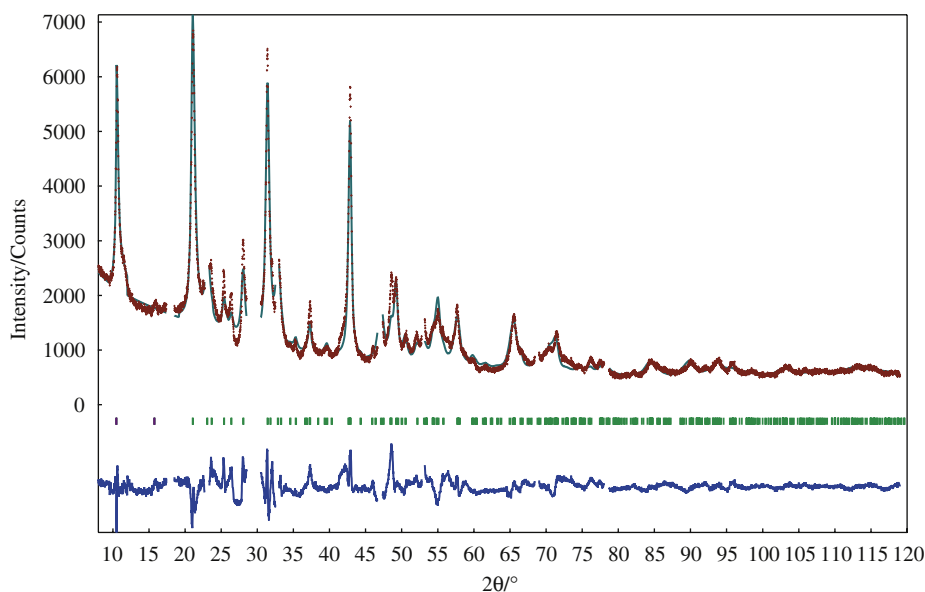


Fig. 7. The Rietveld refinement pattern for the self-assembled sample $KCa_2Nb_3O_{10} \cdot 1.3H_2O$. Observed (red crosses), calculated (smooth green line) and their difference (blue trace). The tick marks indicate the positions of allowed Bragg reflections.

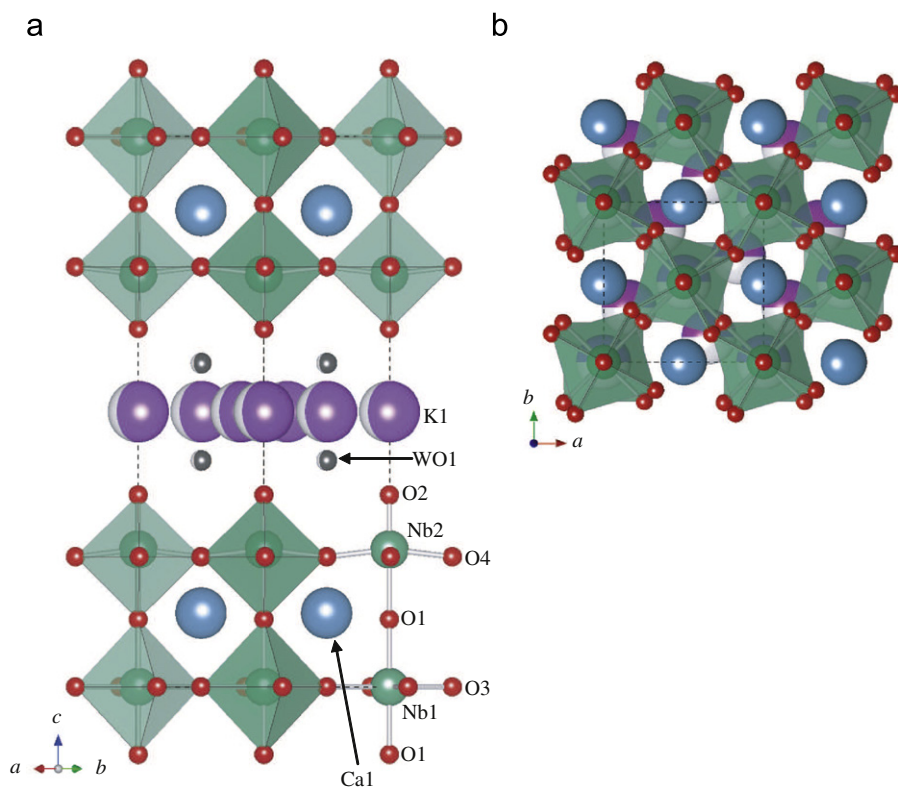


Fig. 8. Polyhedral representations of $KCa_2Nb_3O_{10} \cdot 1.3H_2O$ in the directions of [110] (a) and [001] (b). The dashed black line indicates the unit cell. Selected interatomic distances (in Å): Nb1–O1, 2.08(2); Nb1–O3, 2.01(2); Nb2–O1, 2.14(2); Nb2–O2, 1.67(2); Nb2–O4, 1.94(4); Nb1–Nb1 and Nb2–Nb2, 3.8552(3); Nb1–Nb2, 4.231(2); and K1–O2, 2.54(2).

axis. Inversely, our result indicates that the nanosheets are very regularly restacked along the c -axis, and the a -/ b -axis of each nanosheet orients in the same direction. In Fig. 9b and d, the weak Debye–Scherrer rings and/or spots on the ring are observable. The reflections might be arisen from some small particles lying on the surface of the large crystals, as observed from the SEM images H-form (Fig. 1b) and self-assembled compound (Fig. 6b).

The restacking of negatively charged nanosheets can be attributed to the static self-assembly [36]. Two types of layered structures have been observed after self-assembly of nanosheets, one with turbostratic structure [18] and another one with azimuthal orientation of the a -/ b -axis of each nanosheet [17]. Nanosheets, the so-called two-dimensional crystals, as building blocks are considered to be more difficult to adjust themselves to form a regular layered structure than small ions or small molecules, because the activation energy to reorient a large sheet must be large once it has attached to another sheet in the wrong orientation [18]. However, the present self-assembled sample

shows the third type, i.e. the nanosheets are well restacked upon each other with the a -/ b -axis of each sheet orienting in the same direction. Observably, the bilayer hydrates in the interlayer may take an important role in the reorientation of the nanosheets.

3.4. Dehydration of self-assembled compound

The dehydration of the self-assembled sample results in weight loss, exhibiting four steps from room temperature to 600 °C as shown in TG curve (Fig. 10a), different from that of H-form sample (Fig. 10b). The weight loss of 0.9%, 1.4%, 1.4%, and 0.5% corresponds, respectively, to the temperature range from room temperature to 100 °C, 100 to 280 °C, 280 to 440 °C, and 440 to 600 °C. The variable-temperature XRD patterns are given in Fig. 11. The diffraction peaks of (110), (200), (220), and (400) have no change (indicated with dashed lines in Fig. 11b), suggesting the layer lattice is retained, whereas other peaks change markedly.

Table 4

Bond length distortion index (D) and bond angle variance (σ^2) for K-form, H-form, and self-assembled compounds

Parameter		$\text{KCa}_2\text{Nb}_3\text{O}_{10}$	$\text{HCa}_2\text{Nb}_3\text{O}_{10} \cdot 0.5\text{H}_2\text{O}$	$\text{KCa}_2\text{Nb}_3\text{O}_{10} \cdot 1.3\text{H}_2\text{O}$
Terminal $\text{Nb}(2)\text{O}_6$	D	0.075	0.059	0.044
	σ^2	71.76	126.99	32.7615
Central $\text{Nb}(1)\text{O}_6$	D	0.035	0.043	0.014
	σ^2	1.97	0	0

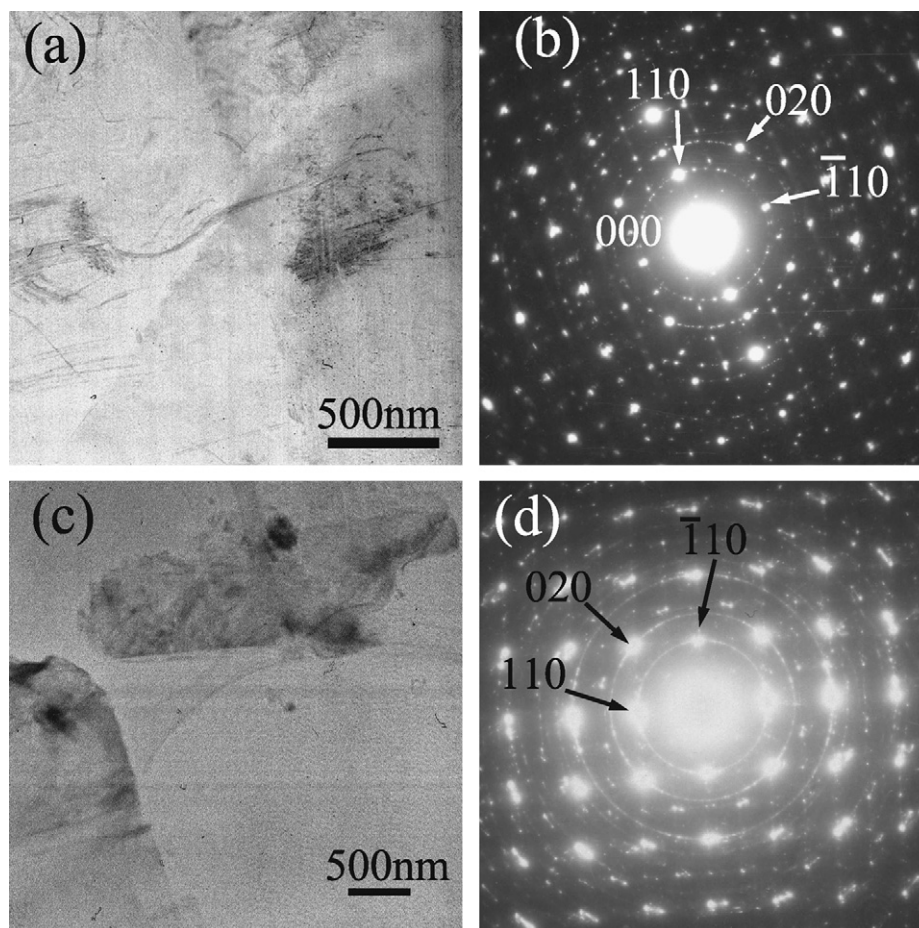


Fig. 9. TEM micrograph and SAED patterns respectively for the self-assembled (a) and (b), and H-form (c) and (d) samples.

The reflection peaks of (00*l*) planes shift to larger 2θ , and the strong peak of (004) plane disappears at 100 °C. Some new peaks attributed to those of the orthorhombic K-form crystals gradually appear as temperature was in excess of 100 °C, and then become sharper and stronger with increasing temperature. As a result, the dehydration process causes the structure change from tetragonal to orthorhombic symmetry. The phase transform agrees with the views that the effect of the K^+ ions on the layers is shielded by the interlayer water molecules, which maintains its tetragonal symmetry as that of the $HCa_2Nb_3O_{10} \cdot 0.5H_2O$.

In the DTA curve (Fig. 10a), the peak at 80 °C shows that the first step of the weight loss (below 100 °C, no symmetry transformation) has marked endothermic effect, and the peak at 405 °C suggests that the symmetry transformation is an exothermal process. The inverse thermal effects happen simultaneously leading possibly to no DTA peak observed between the two temperature ranges.

According to the amount of weight loss, the x value in the $KCa_2Nb_3O_{10} \cdot xH_2O$ formula could be calculated. The relationship of water content and proposed interlayer structure models is shown in Table 5. The d_{basal} change as well as the weight loss vs. temperature is drawn in Fig. 12. During the first weight loss, the d_{basal} kept as a constant 16.44 Å at temperatures below 80 °C and decreased suddenly to 15.68 Å from 80 to 100 °C, showing the interlayer gallery changing from that of K^+ ions solved by bilayer water molecules to an intermediate phase with d_{basal} being ca. 15.6 Å, which is composed of bilayer hydrates but K^+ ions are not well solved. Further dehydration does not markedly make d_{basal}

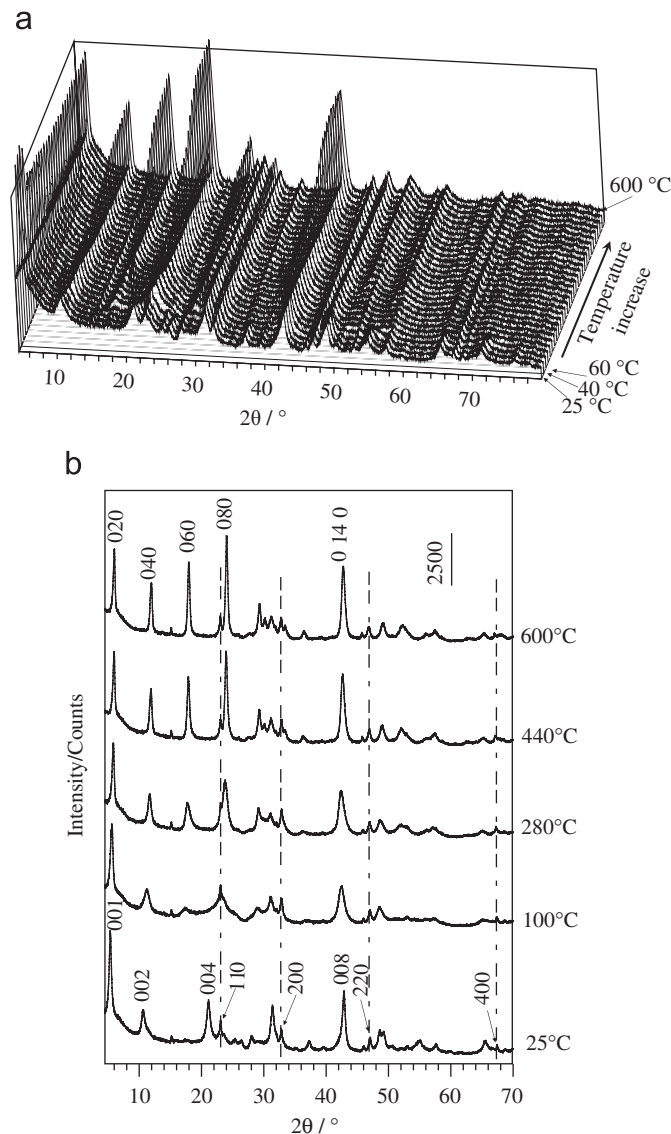


Fig. 11. (a) 3D and (b) expanded XRD patterns of the self-assembled sample recorded at variable temperatures.

decrease till 200 °C. From 200 to 280 °C, the intermediate phase changes to monolayer hydrate. Further till 440 °C, the water molecules of monolayer hydrate are lost, while there is a plateau of $d_{\text{basal}} = 15.0 \text{ \AA}$. At higher temperatures up to 560 °C, the monolayer further loses water molecules, while a d_{basal} plateau of 14.7 Å is observed. Conclusively, the four d_{basal} plateaus indicate that the dehydration unnecessarily changes interlayer distances, and the d_{basal} would persist within a range of water contents and vary markedly once water content is out of the range.

3.5. FT-IR spectroscopy

The FT-IR spectra of the K-form, H-form, and self-assembled samples are shown in Fig. 13, respectively. No vibration band concerning TMA^+ can be found in the spectrum of the self-assembled sample. The bands at 924, 771, and 587 cm^{-1} for the K-form sample (Fig. 13a) are assigned to the stretching vibrations of Nb–O_{terminal} vibrations [37,38], asymmetric stretching vibration of Nb–O_{bridge} in terminal NbO_6 octahedron [39], asymmetric stretching vibration of Nb–O_{bridge} in central NbO_6 octahedron

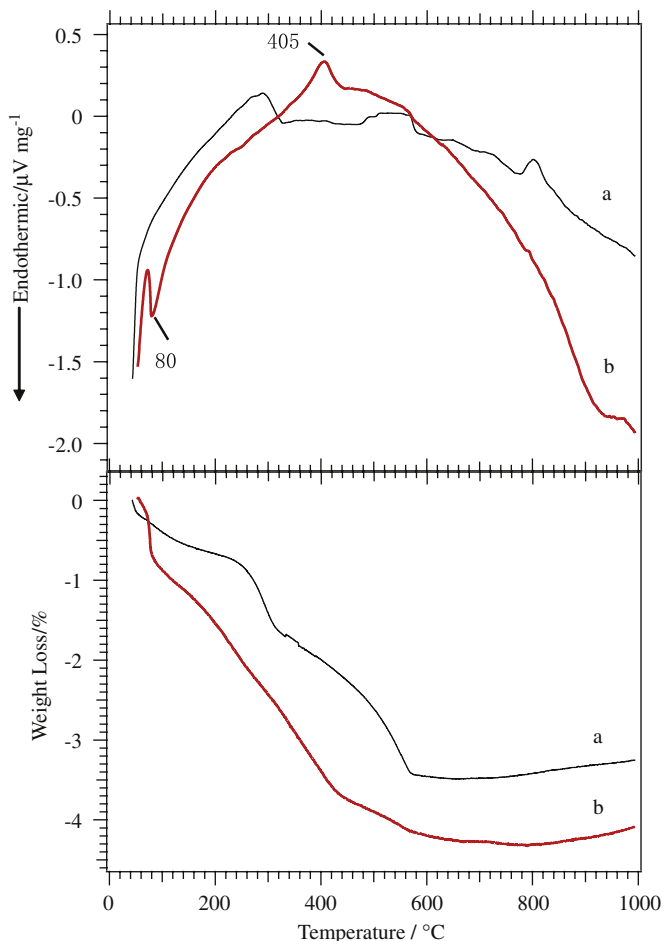
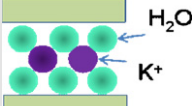
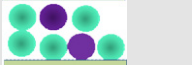





Fig. 10. TG-DTA curves for the self-assembled sample (a) compared with H-form (b).

Table 5
Chemistry formulae ($\text{KCa}_2\text{Nb}_3\text{O}_{10} \cdot x\text{H}_2\text{O}$) and structure models for self-assembled compound at various temperatures

Temperature ($^{\circ}\text{C}$)	Weight loss (%)	x Values	Basal spacing (\AA)	Structure model
25	0	1.3	16.44	
100	0.9	1.0	15.68	
280	2.3	0.6	15.05	
440	3.7	0.2	14.75	
600	4.2	0	14.66	

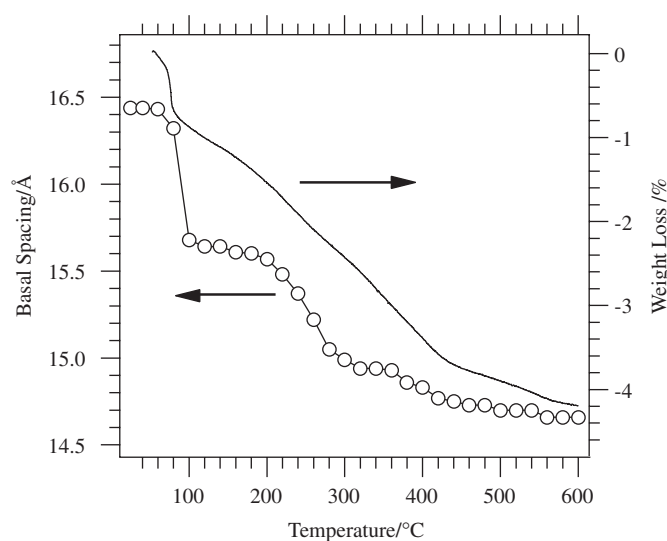


Fig. 12. Plots of the changes of the basal spacings from Fig. 11 and the weight loss from Fig. 10 vs. temperatures.

[37,39], respectively. The band 924cm^{-1} is split to two bands at 948 and 903cm^{-1} for H-form (Fig. 13b). This may be explained as that because protons exist in the interlayer with two types of H^+ and H_3O^+ , the various interaction of H^+ and H_3O^+ with the terminal O atoms results in the different Nb– $\text{O}_{\text{terminal}}$ bonds. For the self-assembled sample, the band at 927cm^{-1} , rather than the split bands, is observed (Fig. 13c), since the considerable increase of water amount and distribution is relatively uniform. For the H-form sample, the bands at 3450 and 1627cm^{-1} are recognized as the stretching and bending vibrations of hydroxyl groups [40]. For the self-assembled sample, the stretching vibration was observed at 3347cm^{-1} . The low wavenumber suggests the elongation of O–H bond because of the interaction of the interlayer K^+ ion and the water molecules. The three bands of Nb–O of the self-assembled sample are sharper and stronger than those of other samples, indicating a smaller distortion of the NbO_6 octahedra. This result coincides with the structure analysis discussed above.

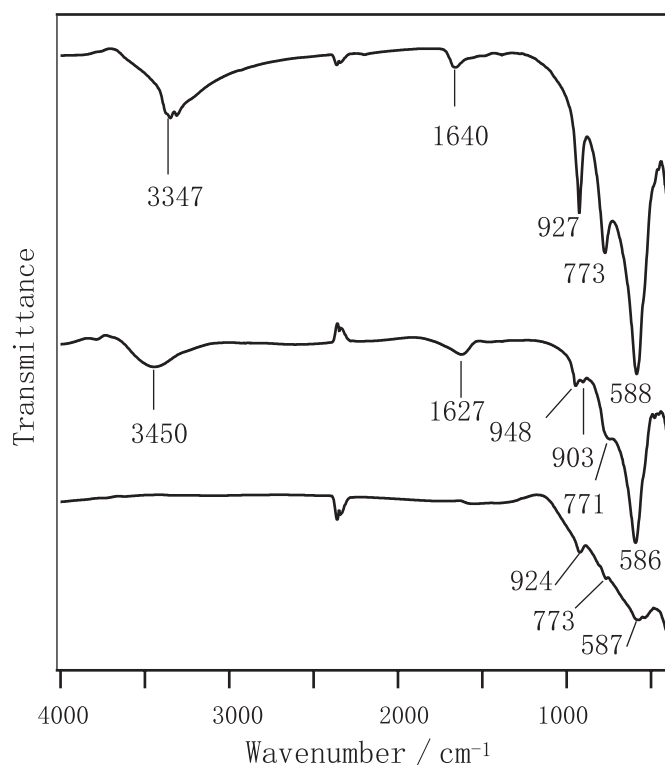


Fig. 13. FT-IR spectra of (a) K-form, (b) H-form, and (c) self-assembled samples.

4. Conclusion

The nanosheets of trilayer perovskite niobate were well restacked to a regular layered structure characterized by the uniform orientations of not only the c - but also a - (and b)-axis of each nanosheet. The self-assembled crystals were tetragonal and have K^+ ions solved by bilayers of water molecules in the interlayer. The space group is the same as the precursor of nanosheets, proton-form niobate. The exfoliation/self-assembly process does not markedly affect the two-dimensional lattice of the layer. Dehydration of the self-assembled compound undergoes

four steps, corresponding to the interlayer gallery change from bilayered hydrates to an intermediate, then to monolayer, and finally to anhydrate. The crystal transformation from trigonal to orthorhombic, the same as the starting material of $\text{KCa}_2\text{Nb}_3\text{O}_{10}$, begins in the second step when temperatures over 100°C and completes in the third step at ca. 440°C .

Acknowledgments

The Project Supported by National Natural Science Foundation of China (no. 20671012) and Post-doctor Science Foundation of China (no. 20070410470).

Appendix A. Supplementary Data

Supplementary data associated with this article can be found in the online version at doi:10.1016/j.jssc.2008.06.014

References

- [1] K. Sakai, T. Motohashi, M. Karppinen, H. Yamauchi, *Thin Solid Films* 486 (2005) 58.
- [2] A. Ulcinas, M. Es-souni, V. Snitta, *Sensor. Actuator. B* 109 (2005) 97.
- [3] (a) H. Jeong, T. Kim, D. Kim, K. Kim, *Int. J. Hydrogen Energy* 31 (2006) 1142; (b) A.S. Dias, D. Carriazo, V. Rives, M. Pillinger, A.A. Valente, *J. Catal.* 244 (2006) 230.
- [4] D. Debasis, G.K. Tanmay, P. Panchanan, *Solid State Sci.* 9 (2007) 57.
- [5] (a) A. Takagaki, M. Sugisawa, D. Lu, J.N. Kondo, M. Hara, K. Domen, S. Hayashi, *J. Am. Chem. Soc.* 125 (2003) 5479; (b) J. Wang, S. Yin, T. Sato, *Mater. Sci. Eng. B* 126 (2006) 53.
- [6] (a) Z.-h. Liu, K. Ooi, H. Kanonoh, W. Tang, T. Tomida, *Langmuir* 16 (2000) 4154; (b) Y. Omomo, T. Sasaki, L. Wang, M. Watanabe, *J. Am. Chem. Soc.* 125 (2003) 3568.
- [7] (a) T. Cassagneau, J.H. Fendler, *Adv. Mater.* 10 (1998) 877; (b) P. Liu, K. Gong, P. Ciao, M. Ciao, *J. Mater. Chem.* 10 (2000) 933.
- [8] Y. Kamiya, N. Yamamoto, H. Imai, S. Komai, T. Okuhara, *Micropor. Mesopor. Mater.* 81 (2005) 49.
- [9] S. Tahara, Y. Sugahara, *Langmuir* 19 (2003) 9473.
- [10] (a) Y.I. Kim, S. Salim, M.J. Huq, T.E. Mallouk, *J. Am. Chem. Soc.* 113 (1991) 9561; (b) A. Kudo, T. Sakata, *J. Phys. Chem.* 100 (1996) 17323.
- [11] N. Miyamoto, K. Kuroda, M. Ogawa, *J. Am. Chem. Soc.* 123 (2001) 6949.
- [12] (a) Y. Ebina, T. Sasaki, M. Harada, M. Watanabe, *Chem. Mater.* 14 (2002) 4390; (b) R.E. Schaak, T.E. Mallouk, *Chem. Mater.* 12 (2000) 2513; (c) R.E. Schaak, T.E. Mallouk, *Chem. Mater.* 12 (2000) 3427; (d) M. Fang, C.H. Kim, G.B. Saupe, H.-N. Kim, C.C. Waraksa, T. Miwa, A. Fujishima, T.E. Mallouk, *Chem. Mater.* 11 (1999) 1526.
- [13] (a) L. Li, R. Ma, Y. Ebina, K. Fukuda, K. Takada, T. Sasaki, *J. Am. Chem. Soc.* 129 (2007) 8000; (b) C. Wang, S. Ye, L. Dai, X. Liu, Z. Tong, *Carbohydr. Res.* 342 (2007) 2237; (c) Y. Zhou, R. Ma, Y. Ebina, K. Takada, T. Sasaki, *Chem. Mater.* 18 (2006) 1235.
- [14] K. Tanabe, S. Okazaki, *Appl. Catal. A: Gen.* 133 (1995) 191.
- [15] M. Sakthivel, W. Weppner, *Sensor. Actuator. B* 125 (2007) 435.
- [16] (a) Y. Ebina, T. Sasaki, M. Watanabe, *Solid State Ion* 151 (2002) 177; (b) F.F. Xu, Y. Ebina, Y. Bando, T. Sasaki, *J. Phys. Chem. B* 107 (2003) 9638.
- [17] X. Yang, Y. Makita, Z. Liu, K. Sakane, K. Ooi, *Chem. Mater.* 16 (2004) 5581.
- [18] X. Yang, Y. Makita, Z. Liu, K. Ooi, *Chem. Mater.* 15 (2003) 1228.
- [19] (a) A.D. Wadsley, *J. Am. Chem. Soc.* 72 (1950) 1781; (b) J. Luo, Q. Zhang, A. Huang, O. Giraldo, S.L. Suib, *Inorg. Chem.* 38 (1999) 6106.
- [20] (a) K. Takada, H. Sakurai, E. Takayama-Muromachi, F. Izumi, R.A. Dilanian, T. Sasaki, *Nature* 422 (2003) 53; (b) K. Takada, M. Osada, F. Izumi, H. Sakurai, E. Takayama-Muromachi, T. Sasaki, *Chem. Mater.* 17 (2005) 2034.
- [21] (a) S. Park, K. Kang, W.-S. Yoon, A.R. Moodenbaugh, L.H. Lewis, T. Vogt, *Solid State Commun.* 139 (2006) 60; (b) S. Park, Y. Lee, M. Elcombe, T. Vogt, *Inorg. Chem.* 45 (2006) 3490.
- [22] V. Thangadurai, W. Wepper, *Solid State Ion* 174 (2004) 175.
- [23] (a) F. Izumi, T. Ikeda, *Mater. Sci. Forum* 198 (2000) 321; (b) H.M. Rietveld, *J. Appl. Crystallogr.* 2 (1969) 63 (c) F. Izumi, <http://www.homepage.mac.com/fujiizumi/index.html>
- [24] (a) M. Dion, M. Ganne, M. Tournoux, *Mater. Res. Bull.* 16 (1981) 1429; (b) A.J. Jacobson, J.T. Lewandowski, J.W. Johnson, *J. Less-Common Met.* 116 (1986) 137.
- [25] H. Fukuoka, T. Isami, S. Yamanaka, *J. Solid State Chem.* 151 (2000) 40.
- [26] The two unindexed peaks was not observed from the self-assembled compound and starting materials $\text{KCa}_2\text{Nb}_3\text{O}_{10}$.
- [27] A.J. Jacobson, J.W. Johnson, J.T. Lewandowski, *Inorg. Chem.* 24 (1985) 3727.
- [28] J. Luo, Q. Zhang, A. Huang, O. Giraldo, S.L. Suib, *Inorg. Chem.* 38 (1999) 6106.
- [29] M.L. Foo, T. Klimczuk, L. Li, N.P. Ong, R.J. CaVa, *Solid State Commun.* 133 (2005) 407.
- [30] V.R. Schöllhorn, *Angew. Chem.* 92 (1980) 1015.
- [31] S.-H. Byeon, H.J. Kim, D.-K. Kim, N.H. Hur, *Chem. Mater.* 15 (2003) 383.
- [32] N.E. Brese, M. O'Keefe, *Acta Crystallogr. B* 47 (1991) 192.
- [33] L. Smith, C. Seith, *J. Magn. Reson.* 179 (2006) 164.
- [34] W.H. Baur, *Acta Crystallogr. Sect. B* 30 (1974) 1195.
- [35] K. Robinson, G.V. Gibbs, P.H. Rabbe, *Science* 172 (1971) 567.
- [36] G.M. Whitesides, B. Grzyowski, *Science* 29 (2002) 2418.
- [37] Y.J. Lu, R. Lalancette, R.H. Beer, *Inorg. Chem.* 35 (1996) 2524.
- [38] (a) K. Saruwatari, H. Sato, J. Kameda, A. Yamagishi, A. Takagaki, K. Domen, *J. Phys. Chem. B* 109 (2005) 12410; (b) V. Katovic, C. Djordjevic, *Inorg. Chem.* 9 (1970) 1720.
- [39] E. Dussauze, E.I. Kamitsos, E. Fargin, V. Rodriguez, *J. Phys. Chem. C* 111 (2007) 14560.
- [40] (b) Y. Narendar, G.L. Messing, *Chem. Mater.* 9 (1997) 580.